The Astrophysical Journal, 673: L191–L194, 2008 February 1


# COMPLEX ORGANIC MATERIALS IN THE CIRCUMSTELLAR DISK OF HR 4796A

John H. Debes,[1] Alycia J. Weinberger,[1] and Glenn Schneider[2]
*Received 2007 October 18; accepted 2007 December 7; published 2008 January 2*

## ABSTRACT

We combine *HST* NICMOS imaging photometry of the HR 4796A disk at previously unobserved wavelengths between 1.71–2.22 $\mu$m with reprocessed archival observations to produce a measure of the dust's scattering efficiency as a function of wavelength. The spectrum of the dust, synthesized from the seven photometric measures, is characterized by a steep red slope increasing from 0.5 to 1.6 $\mu$m followed by a flattening of the spectrum at wavelengths >1.6 $\mu$m. We fit the spectrum with a model population of dust grains made of tholins, materials composed of complex organic materials seen throughout the outer parts of our solar system. The presence of organic material around a star that may be in the later stages of giant planet formation implies that the basic building blocks for life may be common in planetary systems.

*Subject headings:* circumstellar matter — stars: individual (HR 4796A)

## 1. INTRODUCTION

HR 4796A is a young (8 Myr) star with a circumstellar debris disk that has been imaged at several wavelengths (Jayawardhana et al. 1998; Koerner et al. 1998; Schneider et al. 1999; G. Schneider et al. 2008, in preparation). Dust in the disk scatters starlight at visible to near-IR wavelengths and emits thermally in the infrared. Both scattered and thermal emission are spatially coincident originating in a <17 AU wide annulus (Jayawardhana et al. 1998; Schneider et al. 1999; G. Schneider et al. 2008; Koerner et al. 1998) 70 AU from the central star. Estimates of the mass of material present in the disk range from $10^{26}$ to $10^{27}$ g (Jura et al. 1993, 1995). The constituent grains assumed to be responsible for the spatially resolved scattered light and thermal emission have radii on the order of a few $\mu$m although unresolved emission at infrared and submillimeter wavelengths require larger grains a few tens of $\mu$m in size to be present (Augereau et al. 1999; Li & Lunine 2003; Wahhaj et al. 2005; Kessler-Silacci et al. 2005). The smaller grains will escape from the HR 4796A system on short timescales implying a reservoir of colliding bodies that exists to fuel the dust production. The characteristics of the HR 4796A disk make it a younger, dustier analog to the Kuiper Belt within the solar system. Studying HR 4796A provides a probe of planet formation processes around a star with a mass and effective temperature significantly different from our own.

The ring structure of the disk was inferred by thermal emission well fit by a single blackbody temperature (Jura et al. 1993, 1998). It was recognized that the disk could contain dust that was not simply made of silicates, but available observations could not usefully constrain the true composition of the dust grains (Augereau et al. 1999; Wahhaj et al. 2005). Mid-IR Keck LWS spectra from 8 to 13 $\mu$m similarly showed a lack of observable silicate lines or other identifying features (Kessler-Silacci et al. 2005). Near-IR scattered light images of the circumstellar dust (Schneider et al. 1999) suggested a red spectral slope at these wavelengths, hinting at a composition similar to that seen around solar system bodies in the Kuiper Belt.

## 2. OBSERVATIONS

In order to measure the reflectivity of the dust, we observed HR 4796A with the Near-Infrared and Multi-Object Spectrometer (NICMOS) on board the *Hubble Space Telescope* (*HST*) (Thompson et al. 1998) using the coronagraph in Camera 2. We used four medium bandwidth filters ($\Delta\lambda/\lambda \simeq 10\%$), F171M, F180M, F204M, and F222M, with $\lambda_c$ = 1.71, 1.80, 2.04, and 2.22 $\mu$m.

All new observations were taken on 2005 May 9 for HR 4796A and HR 4748, a PSF reference. The observations include direct images of both stars with short exposures for stellar photometry, as well as longer exposures for coronagraphic high-contrast imaging. The instrumentally calibrated and reduced images were created from the raw NICMOS *multiaccum* exposures following the processing methodology described in § 3 of Schneider et al. (2005) and references therein. In addition, we took archival raw images in the STIS 50CCD ($\lambda$ = 0.585 $\mu$m), NICMOS F110W ($\lambda$ = 1.1 $\mu$m), and F160W filters ($\lambda$ = 1.6 $\mu$m) and rereduced the images.

For each of the medium bandwidth filters we directly measured HR 4796A and HR 4748's flux densities with their uncertainties to obtain wavelength-dependent brightness ratios for PSF subtraction. Due to the (detector saturating) brightness, unocculted stellar images were not available in the broader passbands. Thus, we estimated the 50CCD, F110W, and F160W photospheric flux densities with synthetic photometry using the CALCPHOT task of the SYNPHOT[3] package in conjunction with Kurucz models tabulated in the SYNPHOT library. We used a solar metallicity, $\log g$ = 4.5 model of a 9250 K star, using a luminosity of 21.1 $L_\odot$ from a best-fit match to HR 4796A based on its parallax from *Hipparcos*, its Tycho-2 *B* and *V* photometry, as well as its 2MASS *J*, *H*, and $K_s$ photometry. For HR 4748 we used data from the same sources to derive a 121 $L_\odot$, $\log g$ = 4.5 model with $T_{\rm eff}$ = 10,250 K. We compared the predicted F171M, F180M, F204M, and F222M photometry with the SYNPHOT values; they agreed to within a few percent of our measured flux densities. We fit the long-wavelength emission from the disk to a single-temperature blackbody and found $T_{\rm eff} = 78 \pm 1$ K and $L_{\rm IR}/L_\star = (4.8 \pm 0.1) \times 10^{-3}$, a useful surrogate for the disk optical depth. Since $L_{\rm IR}/L_\star \ll 1$, it is reasonable to assume that the disk is optically thin. However, if the ring had a small enough scale height, the disk's radial optical depth would approach unity. We discuss the implications of a radially optically thick disk on our proposed model in § 3.

In order to determine the best subtraction we minimized a $\chi^2$ metric on a region of the diffraction spikes for the target star. We

[1] Department of Terrestrial Magnetism, Carnegie Institution of Washington, Washington, DC 20015.
[2] Steward Observatory, University of Arizona, Tucson, AZ 85721.

[3] See http://www.stsci.edu/resources/software_hardware/stsdas.

TABLE 1
PROPERTIES OF THE HR 4796A DISK

| Filter | Scaling[a] | Flux Density (mJy) | Total Disk Flux Density (mJy) | NE : SW Ratio | $g$ |
|---|---|---|---|---|---|
| STIS 50CCD ..... | 0.705 | 5.5 ± 0.2 | 9.4 ± 0.8 | 0.74 ± 0.07 | 0.16 ± 0.06 |
| F110W ..... | 0.78 ± 0.03 | 5.2 ± 0.3 | 8.1 ± 0.6 | 0.9 ± 0.08 | 0.06 ± 0.07 |
| F160W ..... | ...[b] | 3.7 ± 0.5 | 5.7 ± 0.9 | 1.0 ± 0.1 | 0.0 ± 0.06 |
| F171M ..... | 0.819 ± 0.007 | 2.8 ± 0.1 | 4.8 ± 0.5 | 0.62 ± 0.08 | 0.3 ± 0.1 |
| F180M ..... | 0.79 ± 0.01 | 2.9 ± 0.1 | 4.7 ± 0.3 | 0.71 ± 0.07 | 0.2 ± 0.1 |
| F204M ..... | 0.79 ± 0.02 | 2.5 ± 0.1 | 4.2 ± 0.2 | 1.02 ± 0.09 | 0.2 ± 0.1 |
| F222M ..... | 0.79 ± 0.03 | 2.1 ± 0.1 | 3.5 ± 0.2 | 1.0 ± 0.1 | 0.1 ± 0.1 |

[a] Ratio of HR 4796A to HR 4748.
[b] No contemporaneous PSF reference, used five different references with different scalings.

assume that good subtraction of the diffraction spikes corresponds to the best subtraction of the PSF within the region of interest (Schneider et al. 2001). We searched within 1 $\sigma$ of our scaling uncertainty and iteratively searched to within 0.1 pixels of the best offsets to get the optimal subtraction between target star and PSF.

To quantify the systematic effects on the photometry, we repeated the subtractions varying the PSF scalings and offsets by $\pm 1$ $\sigma$ from the minimum $\chi^2$ solution found above. Using an elliptical photometric aperture matched to the size and shape of the disk, we found the standard deviation in the disk flux densities from this suite of subtractions and used this as a systematic uncertainty per pixel that was then propagated into the disk photometry.

We observed HR 4796A in each medium band filter at two celestial orientations differing by 26°. This is essentially an azimuthal dither that allows true objects that rotate with the field of view to be distinguished from rotationally invariant instrumental artifacts. The two differentially oriented PSF-subtracted images in each filter band were geometrically rectified and corrected for the linear optical distortion ($X_{\rm scale}$ = 75.95 mas pixel$^{-1}$, $Y_{\rm scale}$ = 75.42 mas pixel$^{-1}$) at the Camera 2 coronagraphic focus. The geometrically corrected image pairs were rotated about the location of the occulted target (as determined through the target acquisition process), then co-aligned to higher precision using the image centroids of a nearby field star common in both images, and, finally, combined by averaging.

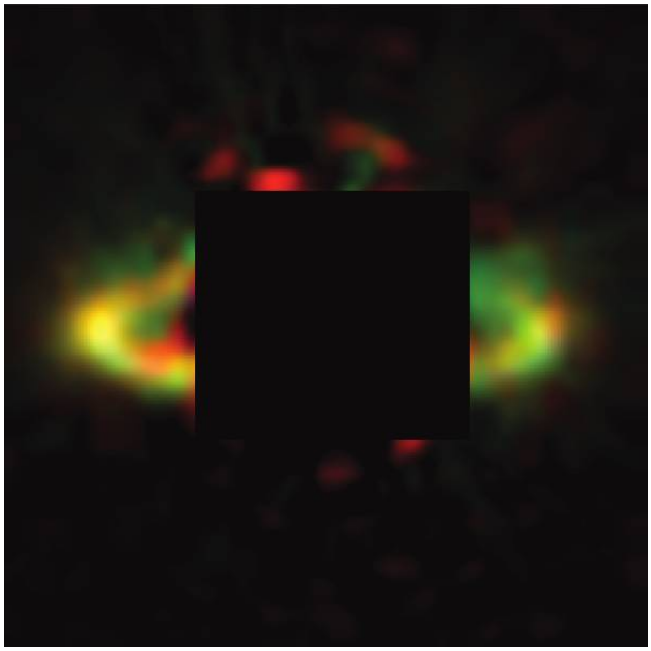

FIG. 1.—False color image of the HR 4796A disk with three of the passbands imaged. Blue corresponds to the 50CCD image, green is the F110W image, and red is the F171M image. A slight color difference between the two lobes of the disk is seen. The central region where PSF subtraction errors dominate is masked out.

To determine the brightness of the disk from the PSF subtracted images, we chose an elliptical aperture with a major-to-minor axis ratio equal to the measured inclination of the disk of 14.1° from edge-on (G. Schneider et al. 2008, in preparation). We used an inner major axis boundary of 0.8″, and an outer major axis boundary of 1.5″. At $r < 0.8''$, systematic errors dominate the image, which restricts useful photometry of the disk to within ±20° of each ansa. Beyond 1.5″, disk flux is below 5%–10% of the peak. We used an elliptical annulus between 1.9″ and 2.5″ with the same azimuthal coverage to determine the background level of the image. Table 1 gives the total measured flux densities of the disk for the four filters.

There were three differences with our rereduction and subtraction of the PSF star for the Cycle 7 F110W and F160W data. We directly calculated pixel centers of the stars behind the coronagraphic hole using the acquisition images and slews reported in the data file headers. A flight software problem caused the relevant header keywords of the acquisition image centroid to be incorrectly populated. The geometric distortion of Camera 2 is time dependent, so we used $X_{\rm scale}$ = 75.87 mas pixel$^{-1}$ and $Y_{\rm scale}$ = 75.19 mas pixel$^{-1}$, appropriate for these observations.

We measured disk asymmetries from our new and reprocessed images, as has been done previously for 50CCD and F110W (G. Schneider et al. 2008, in preparation; Augereau et al. 1999). The disk appears to be asymmetric about the major axis, in a manner consistent with forward scattering dust grains. We quantify this asymmetry in the context of the Henyey-Greenstein $g$-parameter. In addition, the northeastern (NE) side of the disk is brighter than the southwestern (SW) side. We present both sets of measurements in Table 1. There is a marginal trend to a larger $g$-value that peaks at 1.71$\mu$m. The asymmetry between the two sides of the disk is particularly strong at 1.71 and 1.8 $\mu$m.

Figure 1 shows a three-color image of HR 4796A using information from the STIS, F110W, and F171M filters to highlight visually the spectrum of the disk and any spatial variations in the spectrum.

To determine the assumed forward scattering asymmetry of the ring, we measured the total flux in the four readily visible quadrants (between 5° and 15° from the major axis) of the disk between 0.8″ and 1.5″, and took a ratio between the front (brighter) and back (dimmer) parts of the NE and SW ansae of the disk. We calculated the same ratios using a Henyey-Greenstein phase function (Henyey & Greenstein 1941) for the disk inclination to determine a best-fit value for the asymmetry $g$ at each wavelength. To measure the brightness asymmetry between

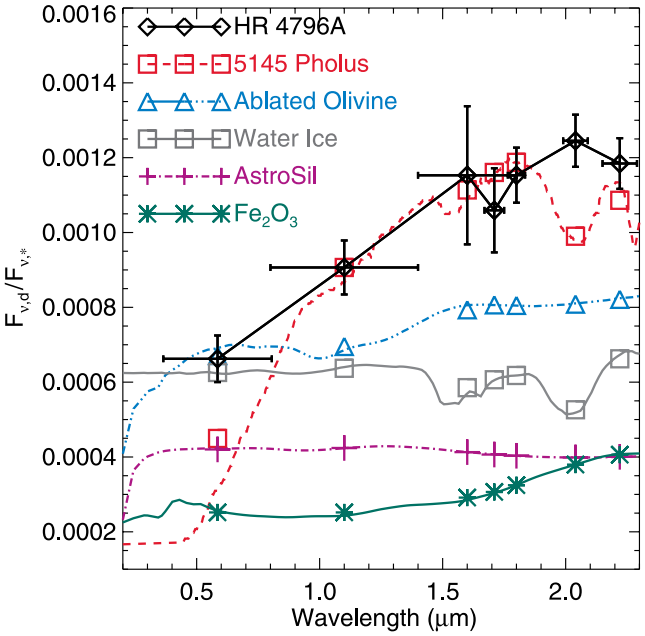


FIG. 2.—$F_{\nu,\mathrm{disk}}/F_{\nu,\star}$ for HR 4796A. Horizontal bars indicate the FWHM of each bandpass. The red curve and symbols represent 5145 Pholus. The other curves represent grain models for candidate materials with an $n^{-3.5}$ size distribution with $a_{\mathrm{min}} = 3$ μm and $a_{\mathrm{max}} = 1000$ μm. Symbols represent the models integrated over each bandpass. Each curve is normalized to the F110W data of HR 4796A and offset for clarity.

the two lobes, we took the total flux in the NE and SW lobes and measured their ratios (±20° from the major axis) between 0.8″ and 1.5″, using the same background annulus.

It is useful to determine how the observed surface brightness in an optically thin disk relates to dust properties. The average surface brightness ($F_{\nu,\mathrm{disk}}/A_{\mathrm{disk}}$) of an optically thin disk is the product of the total scattering cross section of the dust integrated over the volume of the disk multiplied by the flux density of the star ($F_{\nu,\star}$) and the phase function of the dust $\Phi(g, \theta)$ (Augereau & Beust 2006; Schneider et al. 2006). Since our observations were close to the ansae, we assumed that the phase function of the dust could be approximated by the Henyey-Greenstein phase function at a scattering angle of ~90° and assuming the median $g$-value for all of the wavelengths. The measured asymmetries may be used to calculate a geometrical factor relating the total disk flux to the observed flux close to the ansae. The geometrical factor was calculated by using an azimuthally averaged radial cut of both lobes of the disk (±20° from the major axis) and by generating a model disk from that measurement. In addition, we multiplied the model disk by a sine function to approximate the observed NE to SW asymmetry. We measured the ratio of the total flux in the model disk to that of the apertures we used to determine the geometrical factor at each wavelength.

## 3. HR 4796A'S DISK SPECTRUM

A combination of the surface brightness and $L_{\mathrm{IR}}/L_{\star}$ in conjunction with Mie scattering models of a given dust distribution and composition can self-consistently provide a measure of the scattering efficiency ($\langle Q_{\mathrm{sca}} \rangle$) of the HR 4796A disk:

$$\langle Q_{\mathrm{sca}} \rangle = 4 \frac{F_{\nu,\mathrm{disk}}}{\langle a^2 \rangle A_{\mathrm{disk}} F_{\nu,\star}} \frac{(1+g^2)^{1.5}}{(1-g^2)} \left( \frac{\int \langle \sigma_{\mathrm{abs}} \rangle F_{\nu,\star} d\nu}{\int F_{\nu,\star} d\nu} \right) \frac{L_{\star}}{L_{\mathrm{IR}}}, \quad (1)$$

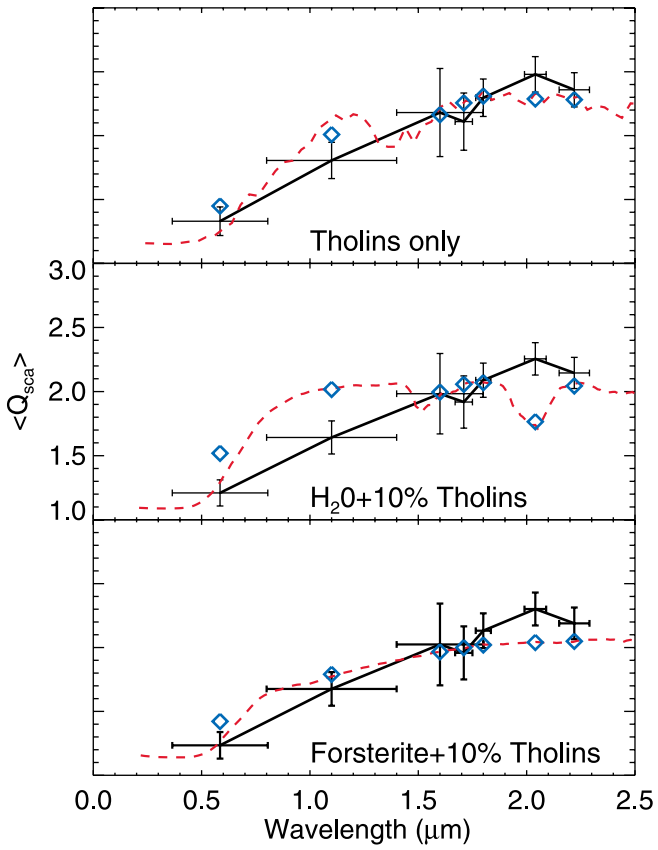


FIG. 3.—Comparison of three models of the dust disk around HR 4796A. *Top*: Tholins with $a_{\mathrm{min}} = 1.4$ μm, $a_{\mathrm{max}} = 980$ μm. *Middle*: Water ice with tholin inclusions that comprise 10% of the volume with $a_{\mathrm{min}} = 12$ μm, $a_{\mathrm{max}} = 100$ μm. *Bottom*: Forsterite with tholin inclusions that comprise 10% of the volume with $a_{\mathrm{min}} = 12$ μm, $a_{\mathrm{max}} = 110$ μm.

where $A_{\mathrm{disk}}$ is the area of the disk, $g$ is the asymmetry parameter for the dust, $\pi\langle a^2 \rangle$ is the effective grain cross section given a power-law dust distribution with a minimum and maximum grain size, and $\langle \sigma_{\mathrm{abs}} \rangle$ is the effective absorption cross section per grain of the dust.

Figure 2 shows $F_{\nu,\mathrm{disk}}/F_{\nu,\star}$ spanning from the visible to the near-IR. The red slope of the disk is reminiscent of organic materials on the surface of Centaur 5145 Pholus but not of other expected components of planetesimals or common red materials such as water ice, astronomical silicates, hematite,[4] or olivine reddened by UV ablation (Cruikshank et al. 1998; Poulet et al. 2002; Laor & Draine 1993; Pollack et al. 1994; Brunetto et al. 2007), also plotted in Figure 2. The scattering properties of organic materials formed in the outer solar system are not well known, but optical constants exist for tholins, complex organic polymers that reproduce the spectral characteristics of organic materials in the atmosphere of Titan and which have been synthesized on Earth (Khare et al. 1984). Tholins have been used to successfully reproduce the red spectra of icy solar system bodies (i.e., Cruikshank et al. 1998). Similar bodies may be colliding to create the dust around HR 4796A.

The top panel in Figure 3 shows a comparison of the disk spectrum with a best-fit grain model of Titan tholins only with two free parameters $a_{\mathrm{min}} = 1.4$ μm, $a_{\mathrm{max}} = 980$ μm, and a fixed power-law index of $\kappa = -3.5$ (Dohnanyi 1969), with a reduced

[4] Optical constants from http://www.astro.uni-jena.de/Laboratory/OCDB/data/oxide/hem_interp.dat.

$\chi^2$ value of the fit of 1.2. The $\chi^2$ contours imply that minimum grain sizes of between 1 and 5 $\mu$m are possible within the 98% confidence contour. The spectrum is weakly dependent on the maximum grain size and so is not a meaningful constraint on the maximum size of the dust. This is true for all the models shown.

Given that the HR 4796A disk's thermal emission can be modeled with a 78 K blackbody, it is conceivable that methane, water, or some other ice may be present in the disk (but see Grigorieva et al. 2007). The spectral shape we see may be due to the presence of tholin inclusions in a larger ice or silicate matrix, since pure ice and silicate models do not possess the red slope seen in the data. Using effective optical constants for water ice with tholin inclusions (Bohren & Huffman 1983) and forsterite with tholin inclusions we compare the resulting $\langle Q_{\rm sca} \rangle$ with our data in Figure 3. The reduced $\chi^2$ values for these two mixtures are 6.8 and 2.0, respectively. These values make an ice+tholin mixture unlikely, but do not rule out the presence of tholin and silicate mixtures.

We note that the general red spectral shape of the disk is very similar to 5145 Pholus, one of the redder objects in the solar system, which is believed to be comprised of water ice with tholin inclusions mixed with olivine and methanol ice (Cruikshank et al. 1998; Poulet et al. 2002). In addition, we confirm that the minimum grain size in our models for the scattered light is comparable in size to the minimum grain size predicted by a detailed fit of the long-wavelength SED (Wahhaj et al. 2005). Tholins provide a useful proxy for the dust present in HR 4796A, but may not be the exact substance observed, given the large number of different compounds that make up tholins.

If, as discussed in § 2, the disk is marginally optically thick in the radial direction, the overall choice of composition would remain unchanged, although the details of grain size and distribution may be different. In a multiple scattering case, the surface brightness of the disk would depend on the extinction efficiency of the dust and $g$ in addition to $\langle Q_{\rm sca} \rangle$. The extinction efficiency and $g$ do not appreciably vary as a function of wavelength between 0.5 and 2$\mu$m for tholin grains. Therefore, even in the case of multiple scattering, the scattering spectrum would depend solely on $\langle Q_{\rm sca} \rangle$. Given that the total mass of dust is uncertain by an order of magnitude and the scale height of the disk is unknown, the optically thin assumption is justified.

The calculations we performed also make strong predictions on the forward scattering behavior of the disk grains. The scattering phase asymmetry parameters predicted by our models for tholin dust are much higher ($g \sim 0.8$) than actually observed (see Table 1). For spherical grains, $g$ is strongly dependent on grain size relative to observed wavelength, and more weakly dependent on composition. The measured asymmetries are much smaller than predicted by our grain model. It is possible that the shape and porosity of the grains make the assumption of spherical symmetry for Mie scattering incorrect and thus markedly changes the phase function of the dust. Porous spherical grains or fractal aggregates tend to have higher $g$-values (Wolff et al. 1998; Bertini et al. 2007), however, so it is not clear what mechanism is responsible for the lower values of $g$ observed. Other disks seem to show low asymmetry (Schneider et al. 2006).

## 4. CONCLUSIONS

We have measured a visible to near-IR photometric reflectance spectrum of the dust ring present around HR 4796A. The scattered light from the ring is suggestive of a grain population dominated by 1.4 $\mu$m radius grains of complex organic material similar in optical properties to the material observed in the atmosphere of Titan and the surfaces of icy bodies in the solar system. The model grains fit the scattered light data but do not fit the observed azimuthal asymmetries in the observed brightness of the dust ring, suggesting that the grains are not spherical.

The library of optical constants for material is not wholly complete, but tholins provide the best fit of the current selection of materials as illustrated in Figure 2. Many minerals and ices can be summarily rejected because they possess relatively neutral scattering efficiencies from 0.5 to 1.5 $\mu$m. UV-ablated olivine has been used to explain particularly red asteroids due to space weathering (Brunetto et al. 2007) and hematite is found on the surface of Mars, but these materials cannot reproduce the observed slope we see in the regime of Mie scattering. Thus, the presence of organic material is the most plausible explanation for the observations.

Longer wavelength scattered light observations will further constrain the grain models we have used, particularly around 3.8–4 $\mu$m, where a large absorption feature is seen for different grain sizes of tholins. This would help to directly confirm whether Titan tholins are an adequate proxy for the material in orbit around HR 4796A. In addition, measuring the optical properties of organic materials in meteorites and from samples of the *Stardust* mission will provide further tests of our model grains.

This research is based on observations with the NASA/ESA *Hubble Space Telescope*, which is operated by the AURA, under NASA contract NAS5-26555. These observations are associated with programs 7233, 8624, and 10167. Support for programs 8624 and 10167 was provided by NASA through a grant from STScI. A. J. W. also acknowledges support from the NASA Astrobiology Institute. J. D. wishes to thank Jeff Cuzzi for insightful conversations on Mie scattering and Alexandra Surcel for a careful reading of the manuscript.

## REFERENCES

Augereau, J.-C., & Beust, H. 2006, A&A, 455, 987
Augereau, J.-C., et al. 1999, A&A, 348, 557
Bertini, I., et al. 2007, A&A, 461, 351
Bohren, C. F., & Huffman, D. R. 1983, Absorption and Scattering of Light by Small Particles (New York: Wiley)
Brunetto, R., et al. 2007, Icarus, 191, 381
Cruikshank, D. P., et al. 1998, Icarus, 135, 389
Dohnanyi, J. W. 1969, J. Geophys. Res., 74, 2531
Grigorieva, A., et al. 2007, A&A, 475, 755
Henyey, L. G., & Greenstein, J. L. 1941, ApJ, 93, 70
Jayawardhana, R., et al. 1998, ApJ, 503, L79
Jura, M., et al. 1993, ApJ, 418, L37
———. 1995, ApJ, 445, 451
———. 1998, ApJ, 505, 897
Kessler-Silacci, J. E., et al. 2005, ApJ, 622, 404
Khare, B. N., et al. 1984, Icarus, 60, 127
Koerner, D. W., et al. 1998, ApJ, 503, L83
Laor, A., & Draine, B. T. 1993, ApJ, 402, 441
Li, A., & Lunine, J. I. 2003, ApJ, 590, 368
Pollack, J. B., et al. 1994, ApJ, 421, 615
Poulet, F., et al. 2002, Icarus, 160, 313
Schneider, G., et al. 1999, ApJ, 513, L127
———. 2001, AJ, 121, 525
———. 2005, ApJ, 629, L117
———. 2006, ApJ, 650, 414
Thompson, R. I., et al. 1998, ApJ, 492, L95
Wahhaj, Z., et al. 2005, ApJ, 618, 385
Wolff, M. J., et al. 1998, ApJ, 503, 815